metals

MDPI

Article

Unlocking the Potential of Sebacate: Investigating Its Role in the Inhibition of Filiform Corrosion on Organic Coated Steel

Andrea Cristoforetti *, Stefano Rossi, Flavio Deflorian and Michele Fedel

Department of Industrial Engineering, University of Trento, via Sommarive n. 9, 38123 Trento, Italy; stefano.rossi@unitn.it (S.R.); flavio.deflorian@unitn.it (F.D.); michele.fedel@unitn.it (M.F.)
* Correspondence: andrea.cristoforetti@unitn.it; Tel.: +39-0461-282403

Abstract: The study investigated the effect of sebacate as a corrosion inhibitor for acrylic-coated steel. Specifically, it examined its impact on mitigating a frequent case of paint delamination, known as filiform corrosion (FFC), through a chosen weathering test designed to stress the degradation of the produced samples. Sebacate was demonstrated to be an efficient organic molecule for enhancing the corrosion resistance of steel. This efficacy was evaluated through electrochemical characterization based on electrochemical impedance spectroscopy measurements and potentiodynamic polarization curves, including the application of an FFC susceptibility prediction methodology based on measurements obtained in FFC-simulated electrolytes. An inhibition efficiency of 98% was measured in near-neutral saline solutions compared to conditions lacking inhibitor presence. During FFC simulation, the primary effect observed was associated with a reduction in cathodic activity evolution. Furthermore, a significant reduction in corrosion creep evolution of 35% was found. These experimental findings aligned closely with the outcomes projected by the simulated investigations.

Keywords: steel; corrosion; corrosion inhibitors; organic coatings; sebacate; filiform corrosion; weathering; material degradation

Citation: Cristoforetti, A.; Rossi, S.; Deflorian, F.; Fedel, M. Unlocking the Potential of Sebacate: Investigating Its Role in the Inhibition of Filiform Corrosion on Organic Coated Steel. *Metals* **2024**, *14*, 623. https://doi.org/10.3390/met14060623

Academic Editor: Jianqiang Wang

Received: 6 May 2024
Revised: 22 May 2024
Accepted: 23 May 2024
Published: 24 May 2024

1. Introduction

Organic coatings are widely employed to safeguard steel substrates from corrosion while preserving their mechanical and functional integrity [1–4]. These coatings typically need to fulfill three primary requirements: adhesion to the substrate, barrier properties against ions and water, and corrosion inhibition [5]. Traditional corrosion inhibitors, often containing chromium (VI) and other toxic compounds, pose environmental and health concerns, necessitating the exploration of safer alternatives [6,7]. Over the years, various environmentally friendly inhibitors have been investigated [8–11], including carboxylic-acid-based molecules known for their ability to form complexes with iron ions, thereby competing effectively with chloride ions [12,13]. Despite their efficacy, the precise mechanism of corrosion mitigation by carboxylates and dicarboxylates remains incompletely understood, although the hydrophobic nature of the resulting thin layer is believed to play a crucial role [14–17]. Notably, the efficiency of carboxylates is influenced by their chain length, with a critical length observed for both mono- and di-carboxylates beyond which their inhibition effectiveness drops significantly due to micelle formation [13,18]. For dicarboxylates on mild steel, there is typically a minor rise in inhibition with increasing chain lengths to a moderate extent. This is succeeded by a rapid escalation to high levels of inhibition, which then experiences a sudden decrease at longer chain lengths [18]. This intricate behavior reflects the simultaneous occurrence of competing processes, including the formation of carboxylate complexes, the adsorption of molecules, and the formation of micelles or hemi-micelles. Hefter et al. [18] depicted a model of the surface interaction mechanism, suggesting that the interplay of these equilibria, potentially complicated further by their kinetics, accounts for the observed effects as chain lengths vary.

Moreover, a correlation was established between corrosion inhibition and the number of carboxylate groups [19]. This study revealed the dependency of the corrosion efficiency of organic molecules containing carboxylate groups on molecular structure features, such as steric effects, electrostatic effects, and electron attractor or donor capabilities.

Carboxylates are classified as non-oxidizing inhibitors, offering corrosion protection in aerated solutions; on the other hand, they demonstrate ineffectiveness in de-aerated solutions [20–22]. This behavior, when dissolved oxygen is present, could be explained by the conversion of anodically generated soluble Fe(II) compounds into the more stable and protective ferric state (Fe(III)). Carboxylates primarily target localized defects within the thin oxide layer, whereby corrosion is mitigated by sealing these defects with corresponding weakly soluble Fe(III) compounds and molecule adsorption in the substrate [23,24]. In this context, a dicarboxylate compound such as disodium sebacate (SB, $C_{10}H_{16}Na_2O_4$), shown in Figure 1, is a suitable candidate to consider. Amidst the pursuit of environmentally benign inhibitors, in recent studies, SB has emerged particularly due to its potential for intercalation in the burgeoning field of a novel type of ceramic-based drug delivery system, namely layered double hydroxides, offering promise as an efficient smart pigment [5,13,25,26]. Thanks to the ion exchange properties inherent in such a lamellar ceramic structure, molecules such as corrosion inhibitors, once intercalated during synthesis or in a subsequent treatment phase, can be accommodated within the structure and gradually released in the presence of other ions, typically chlorides [27]. However, their effectiveness in mitigating the specific yet common paint failure known as filiform corrosion (FFC) [28] remains largely unexplored. This lacuna persists even though the delamination mechanism underlying FFC stems from a combination of distinct reactions and chemical environments at the metal–paint interface [29,30]. Consequently, a targeted investigation is warranted, as the performance metrics derived from cathodic delamination tests, adhesion assessments, and water permeation studies may not be directly applicable to this particular case study. FFC progresses through an anodic undermining process at the metal–paint interface, driven by differential aeration cell formation along the filament's length [31]. This phenomenon is influenced by factors such as humidity levels, coating defects, intermetallic particles, and oxygen availability [32,33]. Conceptually, FFC can be viewed as an electrochemical process characterized by spatially distinct anodic and cathodic regions along the threads [34,35]. The progression of FFC is driven by a potential difference (ΔE_{FFC}), with current density ($i_{CORR\ FFC}$) indicative of its propagation. While FFC usually does not affect structural integrity, it causes severe paint detachment. This compromises the protective coating and can lead to further general corrosion.

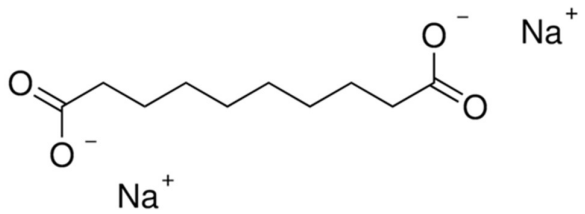

Figure 1. Representation of disodium SB structure.

This study seeks to explore the effectiveness of SB as a corrosion inhibitor for preventing FFC in acrylic-coated steel substrates. Initially, a comprehensive inhibitor evaluation involving chemical and electrochemical analyses, such as Fourier transform infrared spectroscopy (FTIR-ATR), potentiodynamic polarization curves (PDPs), and electrochemical impedance spectroscopy (EIS), was conducted. Subsequently, a detailed investigation into preventing anodic undermining failure was undertaken. The necessity of these assessments arises from the need to comprehensively understand the efficacy of SB in corrosion prevention, particularly in the context of FFC on organic-coated steel, which has remained understudied. Additionally, this study introduces a novel electrochemical

simulation method to evaluate the inhibition efficiency specifically for FFC, with the results validated by observing actual corrosion creep development during humidostatic weathering tests. The corrosion mechanisms can vary notably between acidic and neutral aqueous environments, largely due to the presence or distinct properties of metal oxide/hydroxide films at elevated pH levels. Consequently, extrapolating conclusions regarding the probable effectiveness of inhibitors in neutral solutions from data acquired in acidic solutions can be misleading or even lead to adverse outcomes.

2. Materials and Methods

2.1. SB Electrochemical Characterization in a Near-Neutral Environment

In the electrochemical characterization of SB, bare R36 Q-Panel Steel A1008 surfaces (composition: C max. 0.15 wt.%; Mg max. 0.6 wt.%; P max. 0.03 wt.%; S max. 0.035 wt.%; and Fe. Bal.) were pickled for 15 min in 2 M HCl, followed by immersion in a 0.5 M NaCl solution containing 3 g/L of SB. An Autolab 302N potentiostat/galvanostat/FRA (Metrohm AG, Herisau, Switzerland) was employed with a three-electrode setup, with the steel panel serving as the working electrode, while platinum and Ag/AgCl/3.5 M KCl electrodes were utilized as the counter and reference electrodes, respectively. EIS spectra were recorded at the open circuit potential (OCP) over a frequency range of 100 kHz to 0.01 Hz, with a signal amplitude of 5 mV (RMS) and 6 points per decade, after 3 h of immersion. The obtained EIS data were analyzed using ZSIMPWIN® 3.50 software to derive equivalent electric circuits (EECs). The PDPs were obtained at a scan rate of 0.2 mV/s, ranging from −50 mV to +700 mV vs. the OCP, following a 3 h wait period.

2.2. Electrochemical Simulated Study on the Inhibition of FFC

Furthermore, to investigate the protective effects of the inhibitor against FFC, PDPs were also collected employing an anolyte/catholyte simulating setup (as described in refs. [5,35]). Also, in this case, 3 g/L of SB powder was introduced into the testing electrolytes. The anodic and cathodic branches of the PDPs were individually collected following a 3 h waiting period, during which the OCP was monitored (Appendix A, Figure A1). The anodic and cathodic branches were acquired through two separate tests by polarizing the system relative to the OCP. The anodic branch ranged from −50 mV to +300 mV, while the cathodic branch spanned from +50 mV to −300 mV. According to the procedure adopted in references [5,35], the anolyte contains 0.1 M $FeCl_3$, as it is expected that some iron dissolution will occur at the anodic site. The pH was adjusted to 1.5 by gradually adding 33% HCl. Recognizing that at the anodic site, the oxygen levels were likely reduced due to limited availability derived from the directionality of the supply through the filaments and the high ionic concentration [29,31], nitrogen was continuously purged into the anolyte to decrease the dissolved oxygen to around 1.4 ppm, measured using a PCE-PHD 1 probe (PCE Instruments, Capannori (LU), Italy). Considering that the cathodic reaction induces localized alkalinization due to the oxygen reduction reaction on the steel substrate ($4Fe^{2+} + O_2 + 2H_2O \rightarrow 4Fe^{3+} + 4OH^-$) [32,33], the catholyte was prepared using a NaOH aqueous solution with a pH of 12 [29,32]. This arrangement was anticipated to promote the passivation of the steel surface [36]. Continuous air bubbling was employed to maintain stable dissolved oxygen levels in the electrolyte.

2.3. Preparation of Acrylic-Coated Steel Samples

The effectiveness of the protective action of the SB was tested on coated steel samples composed of steel panels painted with two layers of a bicomponent polyamide-based clearcoat (supplied by Palini Vernici, Pisogne, BG, Italy). The primer layer was loaded with SB at a concentration of 1 wt.%. The top coat was a simple paint-covering layer (the same base composition as the primer) to avoid possible leaching of the particles toward the outer side of the coating. The steel substrate was initially cleaned by degreasing it with acetone under ultrasonic treatment. Subsequently, the surface was pickled in a 2 M HCl

acid solution for a duration of 15 min. Paint was applied using the automatic applier Elcometer 4340 (Manchester, UK) to deposit 100 μm of wet thickness for each layer. Each layer applied underwent curing at 60 °C for 1 h, reaching a total dry thickness of 75 μm. To promote uniform dispersion of the pigments and prevent agglomeration after mixing them into the liquid paint, an ultrasonication step was conducted for a period of 10 min.

2.4. Characterization and Aging of Acrylic-Coated Steel Samples

Three painted samples of each type were aged following ASTM standard 2803 [37] to observe the spread of the FFC. A 45 mm long and 1 mm wide scratch was created on each specimen. The coated panels were protected with adhesive tape to avoid early cut-edge failure. Initially, a 5 h contamination stage in a neutral salt spray chamber [38] was conducted before subjecting the specimens to 750 h of humidostatic aging. During the aging process, the temperature was maintained at a constant 40 °C, and the relative humidity was set at 80%.

Similar coated plates were immersed in a NaCl solution (0.5 M) for 500 h. The coating system was monitored periodically by recording the EIS response. Spectra were recorded at room temperature (25 °C) in an aqueous solution with a quasi-neutral pH (6.2) and with 7.5 ppm dissolved oxygen, measured using a PCE-PHD 1 probe (PCE Instruments, Capannori (LU), Italy). The spectra were recorded at a voltage amplitude of ±15 mV with respect to the open circuit potential in a frequency range from 0.01 Hz to 100 kHz. A built-in-house mobile cell with a platinum counter electrode with an area of 0.75 cm^2 and an Ag/AgCl/3.5 M KCl reference electrode with a planar circular test area of 9 cm^2 was used as the working electrode. EIS data collection was performed to evaluate the corrosion protection properties of the paint during the development of the degradation of the coating system and the activation of the pigments loaded in the primer layer; each sample was analyzed periodically.

3. Results

3.1. SB Effect Characterization

From an electrochemical point of view, the SB's behavior in near-neutral conditions highlighted enhanced corrosion resistance, both in the PDPs and EIS. Comparing the outcomes with a reference case of blank saline solution (Ref.), SB's adsorption, with the formation of insoluble compounds on the surface [23,24], provided notably higher corrosion potentials and decreased the current densities by two orders of magnitude (Figure 2a) when the sample was anodically polarized. The difference in the OCP is comparable in the case of the cathodic branches of the PDPs, although concerning the cathodic activity current density, the inhibitor showed similar values to the reference curve (Figure 2b). On average, the steel substrate undergoing interaction with the SB experienced an increase in its OCP of +0.46 ± 0.09 V. These results are consistent with the information reported in the literature regarding specific cases of using SB as an inhibitor for steel, confirming its classification as an anodic inhibitor when tested in a nearly neutral aqueous environment [13,26].

On the other hand, the impedance modulus at low frequencies increased by more than one order of magnitude (Figure 2c). The changes at the metal interface were evaluated according to EEC analysis utilizing an R(QR) circuit, where Q stands for a constant-phase element (CPE) suitable for taking into account the deviations from the ideal capacitive behavior of the electrical double layer. Its definition, according to Equation (1), involves the parameters of the pre-exponential Y_0 and the exponent n, the values obtained for which are reported in Table 1. Moreover, the remaining parameters extracted were attributed to the electrolyte and the polarization resistance (R_s and R_{ct}), from which an index representative of the inhibition efficiency could be calculated [26,39] following Equation (2). Thanks to the higher magnitude of R_{ct} when SB was involved, the inhibition stood at around 98% in this case study and placed SB as one of the most successful

inhibitors within the field of organic compounds [26,40]. In conjunction with a higher impedance modulus at low frequencies, SB's presence significantly impacts the EIS spectrum by broadening the time constant of the phase angle at medium to low frequencies, testifying to changes in the structure of the double layer at the metal interface.

$$Q(\omega) = [Y_0(j\omega)^n]^{-1}, \quad (1)$$

$$IE\% = (R_{ct} - R_{ct0})/R_{ct}, \quad (2)$$

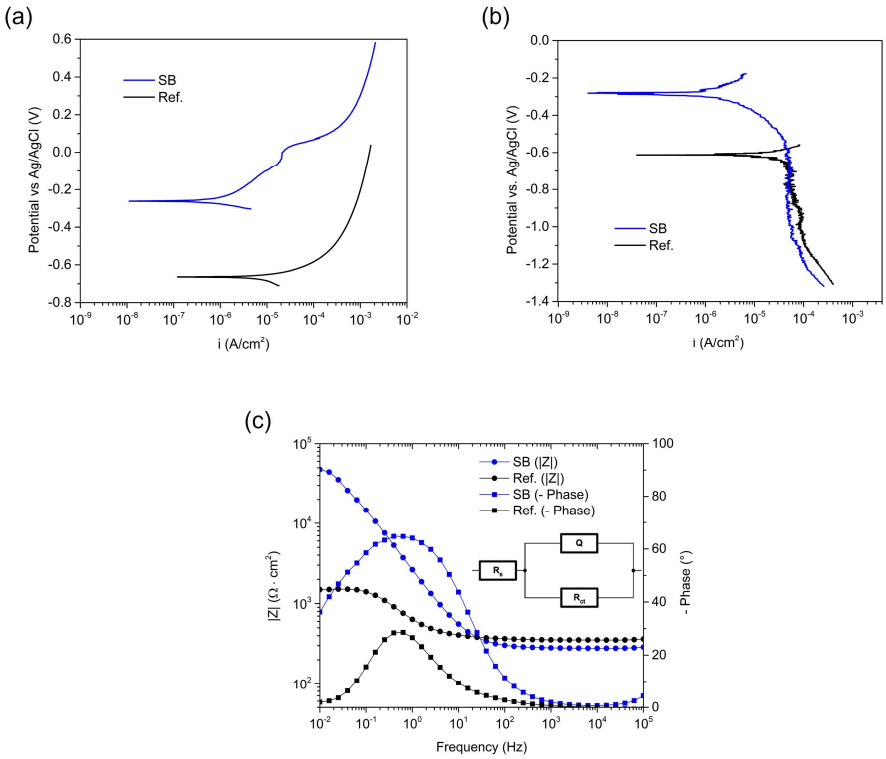

Figure 2. Anodic (**a**) and cathodic (**b**) polarization curves and Bode representation of EIS spectra (**c**) obtained following 3 h of immersion in 0.5 mol/L NaCl solution for bare steel surfaces with and without addition of 3 g/L SB. The inset shows the R(QR) EEC adopted for the spectra modeling.

Table 1. Outcomes of EIS data analysis utilizing the electrochemical equivalence model R(QR).

Sample	R_{ct} ($\Omega \cdot cm^2$)	Y_0 ($S \cdot cm^{-2} \cdot s^n$)	n	R_s ($\Omega \cdot cm^2$)	IE%
Ref.	1.21×10^3	5.45×10^{-4}	8.14×10^{-1}	3.75×10^2	-
SB	6.25×10^4	8.99×10^{-5}	8.08×10^{-1}	2.97×10^2	98

3.2. Prediction of FFC Mitigation Using an Electrochemical Simulated Method

An electrochemical setup to simulate the head and tail of an FFC filament was employed to collect PDPs for the anolyte and catholyte to assess the potential of the synthesized particles to inhibit FFC propagation (Figure 3). In comparison to the polarization curves presented in Figure 2a,b, the anodic and cathodic branches collected in diverse electrolytes could better distinguish the precise contribution of the inhibitor in the specific simulating environment. This approach allowed for the evaluation of the inhibitive effect in terms of the FFC corrosion current ($i_{CORR\ FFC}$), which is determined at the intersection point between the anodic and cathodic branches, as well as the potential difference between the anodic and cathodic sites (ΔE_{CORR}). The output of the measurements is reported

in Table 2 for the two different cases under investigation. The curves displayed revealed intriguing outcomes, demonstrating a reduction in ΔE_{CORR} in the order of 87% caused by the presence of SB. The inhibitor's contribution turns out to be overwhelming, acting mainly on the cathodic activity. Besides the shift in the cathodic curve, a decrease in $i_{CORR\ FFC}$ of one order of magnitude is caused by the organic inhibitor's adsorption onto the steel surface. The addition of the inhibitor to the anolyte environment does not yield a significant effect, likely attributable to the aggressive acidic conditions and the lower oxygen content (1.4 ppm [35]). These findings support the characterization of carboxylate inhibitors as non-oxidizing agents, primarily effective in aerated conditions, such as those present in the considered catholyte. Furthermore, the results elucidate how the characterization of the inhibitor's effectiveness, discerned as primarily anodic through electrochemical assessments in nearly neutral solutions and in the literature [13], is contingent upon the specific physicochemical conditions in which it operates. Regarding the presented curves' reproducibility, replicas are provided in Appendix A, Figure A2.

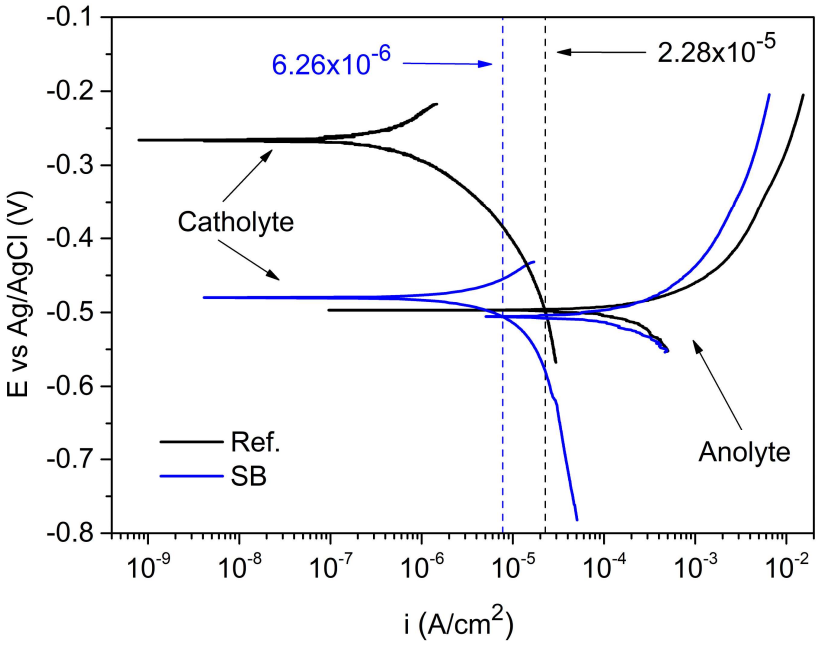

Figure 3. PDPs collected on bare steel surface using anolyte and catholyte "Ref." and with 3 g/L of SB added. The numerical values (expressed in A/cm²) of FFC corrosion current as the intersection between anodic and cathodic branches are reported.

Table 2. Electrochemical parameters estimated from the electrochemical simulated approach.

Sample	Inhibitor Addition	$i_{CORR\ FFC}$ (A/cm²)	ΔE_{CORR} (V)
Ref.	-	2.28×10^{-5}	0.230
SB	3 g/L	6.26×10^{-6}	0.030

3.3. Acrylic-Coated Steel's Durability

The coated steel samples underwent testing to compare the corrosion evolution of organic layers loaded with SB with those with a neat acrylic coating. FFC tests were conducted under static conditions at 80% relative humidity and 40 °C, revealing a reduction in corrosion propagation from artificial scratches, as depicted in Figure 4. The occurrence of coating delamination, resulting from blister formation and filiform propagation, was observed to be mitigated by the presence of SB within the coating. This is attributed to

SB's capacity to migrate through the coating and effectively reach the metallic surface. Notably, discernible disparities in the degradation morphology were observed among the samples, with FFC representing the initial coating detachment event, succeeded by a broader blistering front encompassing the entire initial defect.

Figure 5 reports the average value of the expansion of the corrosion-damaged area around the scratch, calculated for three replicates of each type of sample. The inhibition degree was determined to be an average reduction of 35% in the corrosion rate (calculated from the slopes of the trends reported in Figure 5, quantified in terms of the expansion of the corroded area by means of the ImageJ 1.53t software thanks to the transparency of the coating). This result is noteworthy, particularly considering the relatively low concentration of the inhibitor (1 wt.%) incorporated into the coating, in comparison with analogous studies documented in the literature [41–43]. The influence of SB becomes more apparent over time, particularly as filaments begin to emerge due to the initial blister-induced paint delamination. This phenomenon is evident in Figure 4, where the damage observed in two types of samples remains comparable until 220 h of weathering. This observation may be attributed to the reasonable period required for the activation and percolation of the inhibitor through the coating to the interface. Consequently, the incorporation of such organic molecules into the coating does not appear to confer a beneficial effect during the initial stages of FFC. Hence, it might be more advantageous to combine these molecules with other mitigation strategies, such as conversion coatings, which exhibit greater efficacy during the initiation phase [5].

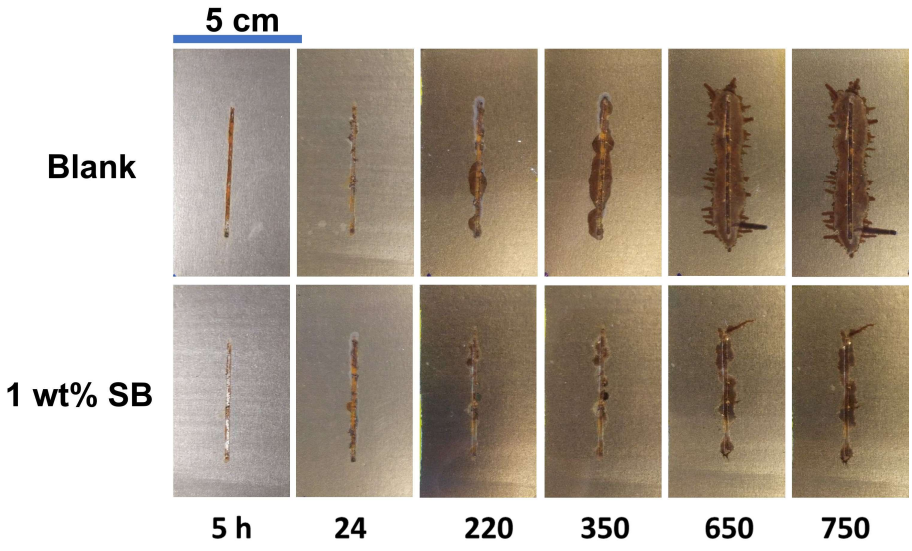

Figure 4. State of corrosion creep of scratched coated samples during 750 h of FFC test at 40 °C in humidostatic conditions (80% r.h.) after 5 h of contamination stage in a neutral salt spray chamber. Acrylic-coated steel panels with (1 wt.% SB) and without (Blank) the addition of the inhibitor are compared.

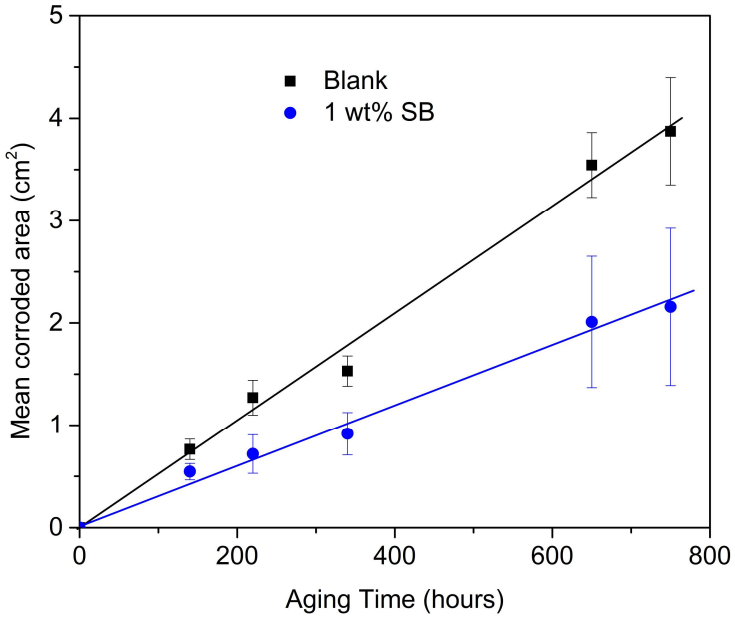

Figure 5. Corroded area evolution over time during 750 h of aging. The mean value calculated for three replicas is reported. Acrylic-coated steel panels with (1 wt.% SB) and without (Blank) the addition of the inhibitor are compared.

To delve deeper into the behavior of the coating system when exposed to humidity penetration, and also to determine whether the presence of the inhibitor adversely affected the barrier properties of the coating, EIS was conducted on coated steel panels immersed in a 0.5 M NaCl solution. Both monitored samples showed a decrease in values at low frequencies, although the starting values and the impedance decay demonstrate better performance in the case of the coating loaded with SB (Figures 6a and 7a). In the case of the presence of SB in the paint, the transition from capacitive to resistive behavior appears to be less pronounced and sharp compared to the reference "Blank" case and is visible in the spectra starting from 336 h of immersion. This trend could be due to the hydrophobic nature of the interfacial layer formed by the deposits of SB, a property that would hinder the kinetics of water absorption within the organic layer. A transient at the middle frequencies is afforded by the inhibitor, likely due to its solubility and the adsorption process at the metal–paint interface. On the other hand, the "Blank" sample showed a net change between resistive and capacitive behavior.

More in-depth study of the various electrochemical contributions that make up the overall behavior of the coating system was achievable through a spectra modeling study using EECs. However, the results obtained in this step, using a typical organic coating R(Q(R(QR))) data analysis circuit, exhibit in some cases trends that are challenging to attribute to physical phenomena. A CPE (namely Q) is employed to account for the non-ideal capacitive behavior of the coating. Q is helpful in this case for correctly modeling the nonlinearity of the solid electrodes, derived from dissipative phenomena in the polymers, the interaction between polar groups, and diffusive processes at the interface [44]; for this purpose, Q is introduced into the circuit, similar to the case of the EIS collected on bare steel, where its impedance is represented in Equation (1). In principle, two contributions can be attributed to the organic coating (incorporating C_{coat} and R_{coat}) and the interface (composed by the double-layer capacitance C_{dl} and the charge transfer resistance R_{ct}), where the inhibitor adsorbed onto the metal surface should impart a distinguishable effect compared to the reference case, particularly in terms of the charge transfer resistance. This last parameter, as shown in Figure 8a, demonstrates that despite an initial likely higher

defectiveness of the "SB" sample, distinguishable from comparison with the reference "Blank" sample, the release of the inhibitor after 150 h of immersion and its subsequent adsorption at the interface provide a healing effect that leads to significantly higher values.

Concerning the other extracted parameters, each interpretation reported in Figure 8 cannot straightforwardly lead to definitive comments on the electrochemical behavior due to the minor differences in values, and therefore any speculation on these parts of the results has been avoided. Only a comparable decrease in the coating resistance R_{coat} for both samples is observed in Figure 8d, indicative of the loss of the barrier properties of the organic layer, together with electrolyte permeation, a feature that does not seem to be altered by the inhibitor's presence in the organic layer.

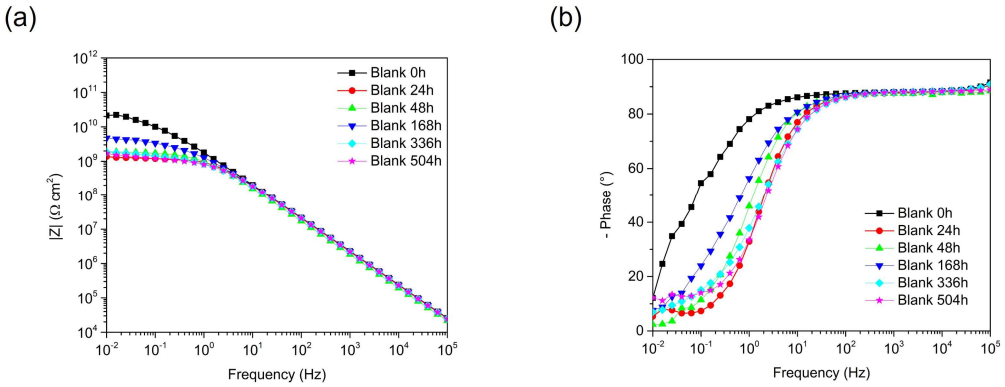

Figure 6. EIS Bode spectra after different immersion periods collected for painted steel samples. Impedance modulus |Z| is reported on the left side (**a**), while a phase angle diagram is shown on the right side (**b**). Blank (neat acrylic paint) behavior is reported during 504 h of immersion in 0.5 M NaCl solution.

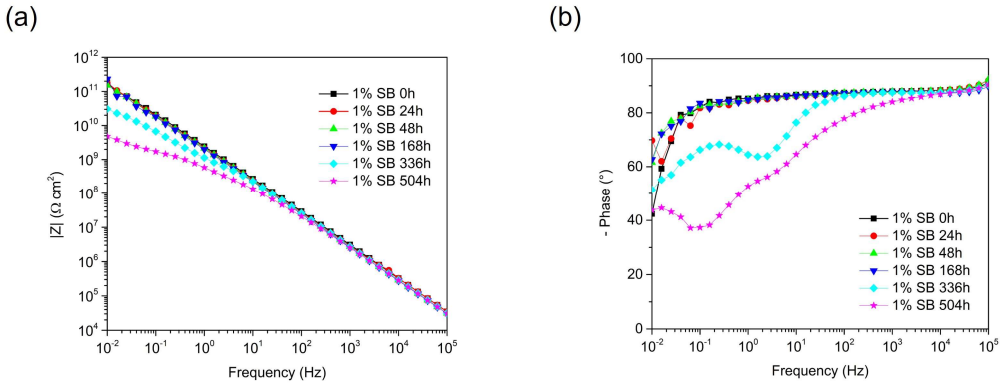

Figure 7. EIS Bode spectra after different immersion periods collected for painted steel samples. Impedance modulus |Z| is reported on the left side (**a**), while a phase angle diagram is shown on the right side (**b**). The behavior of the coating loaded with 1 wt.% SB is reported during 504 h of immersion in 0.5 M NaCl solution.

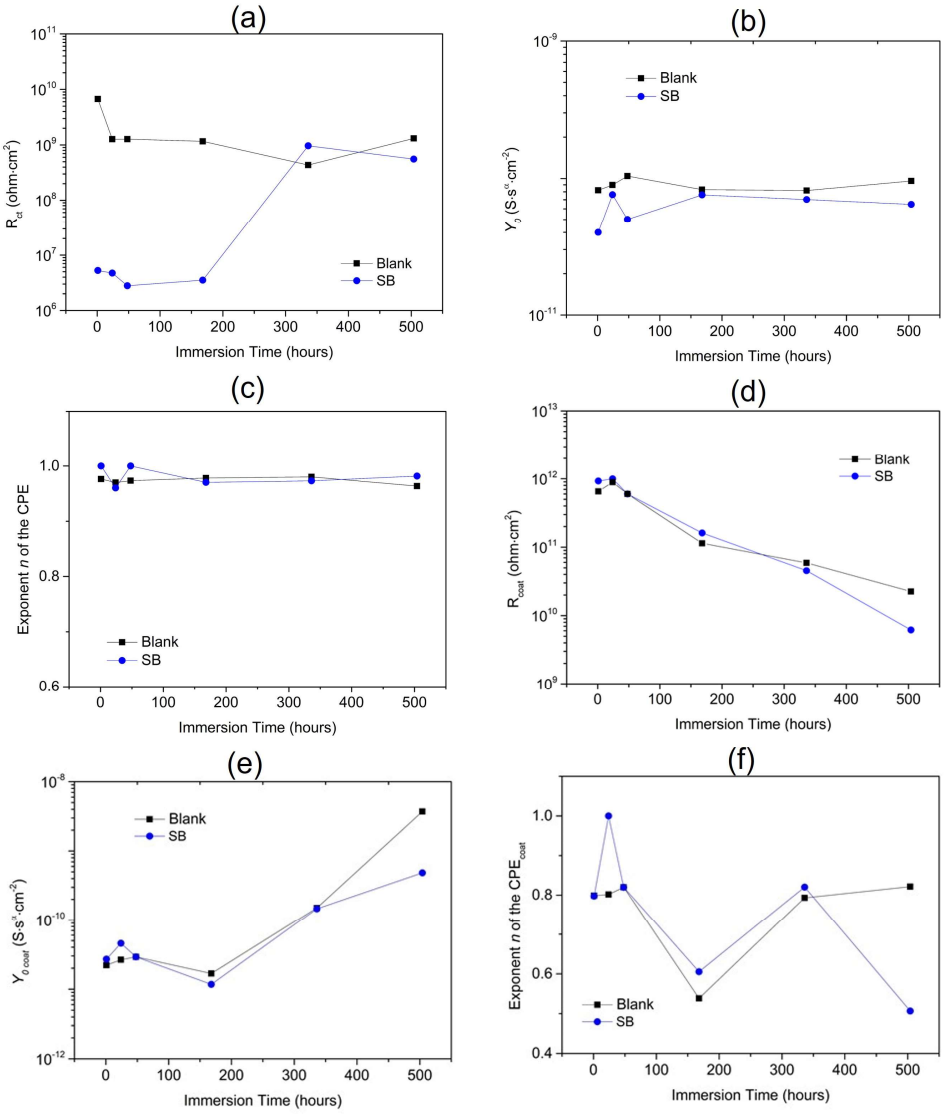

Figure 8. Results of the EIS fitting over testing time. The contributions attributed to the Faradaic processes (**a**–**c**) and the coating are reported (**d**–**f**).

4. Discussion

The results unanimously support attributing effective inhibitory power to SB when it is employed on painted steel. It is well known that different corrosion mechanisms lead to varied durability performances for similarly coated substrates, depending on the surrounding environmental conditions, particularly influenced by humidity levels and the presence of contaminant ions. In this study, such evidence is underscored by electrochemical tests based on EIS measurements and PDPs. The diverse chemical composition of the electrolytes used, along with the levels of oxygen present in the solution, resulted in different contributions that the molecule under study made to the evolution of the electrochemical environment at the metal interface. Specifically, SB, known as an anodic inhibitor [13,26], as verified in this study (Figure 2), markedly influences the cathodic activity when an aerated solution exhibits high alkalinity (Figure 3). This scenario occurs in real-life situations where FFC propagates beneath the coating. Consequently, it can be asserted that a singular classification of corrosion inhibitor behavior is not exhaustive, and this

characteristic must be related to and studied not only considering the specific case of use, such as organic coatings being exposed in an outdoor environment but also, above all, considering the actual degradation mechanism at play. The choice of an appropriate inhibitory substance should be informed by a detailed understanding of the specific degradation mechanism at play. In the context of preventing coating delamination, it is essential to consider the reactions at the extending front. While some strategies may offer general metal protection irrespective of the corrosion mechanism, others are more tailored to specific phenomena, such as FFC, which is cathodically nucleating and typically exhibits anodic delamination. The selection of a mitigation pathway is therefore contingent on the intricacies of the corrosion process. In the specific case of SB, this substance appeared to be effective in both delamination scenarios, but this is not necessarily a generalizable example and specifically concerns the stability of molecules at different pH levels and their interaction with the metallic substrate in such environments.

5. Conclusions

In this study, we investigated the potential of an eco-friendly organic corrosion inhibitor, namely SB, particularly in the context of acrylic-coated steel. Preliminary electrochemical analyses significantly contributed to our understanding of its inhibitive properties, particularly concerning mild steel in near-neutral conditions. SB is confirmed to act as an anodic corrosion inhibitor under nearly neutral conditions, and electrochemical tests in simulated environments highlight its efficiency in aerated conditions, like other carboxylic acids. In these conditions, an inhibitory effectiveness of 98% was seen compared to situations where the inhibitor was absent.

Additionally, SB has also been shown to limit cathodic activity, specifically in the case of an alkaline, aerated environment, typical of cathodic sites involved in the phenomenon of FFC for coated steel. At this stage, to predict its actual effect on degradation due to FFC, we employed a predictive approach, utilizing electrochemical simulations. This involved analyzing the PDPs of bare steel immersed in test solutions designed to mimic the unique environment anticipated at the metal–paint interface. These simulations yielded results that closely aligned with the observed performance of the coated steel. Specifically, the presence of the inhibitor (referred to as "SB") in the primer layer demonstrated notable limitations in paint delamination and corrosion expansion to 35%.

Author Contributions: Conceptualization, A.C., S.R., F.D., and M.F.; methodology, A.C. and M.F.; software, A.C.; validation, S.R., M.F., and F.D.; formal analysis, A.C., M.F., and S.R.; investigation, A.C.; resources, M.F., S.R., and F.D.; data curation, A.C.; writing—original draft preparation, A.C.; writing—review and editing, A.C., M.F., S.R., and F.D.; visualization, A.C., S.R., F.D., and M.F.; supervision, S.R., F.D., and M.F.; project administration, S.R., F.D., and M.F.; funding acquisition, S.R., F.D., and M.F. All authors have read and agreed to the published version of the manuscript.

Funding: This research received no external funding.

Data Availability Statement: The raw data supporting the conclusions of this article will be made available by the authors upon request.

Acknowledgments: The authors gratefully acknowledge Palini Vernici (Pisogne, BG, Italy), in particular Sergio Bartolomeo.

Conflicts of Interest: The authors declare no conflicts of interest.

Appendix A

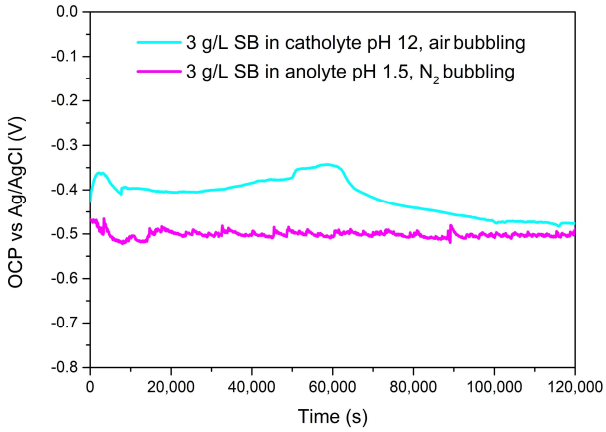

Figure A1. OCP of bare steel immersed in anolyte and catholyte monitored over time with addition of 3 g/L SB.

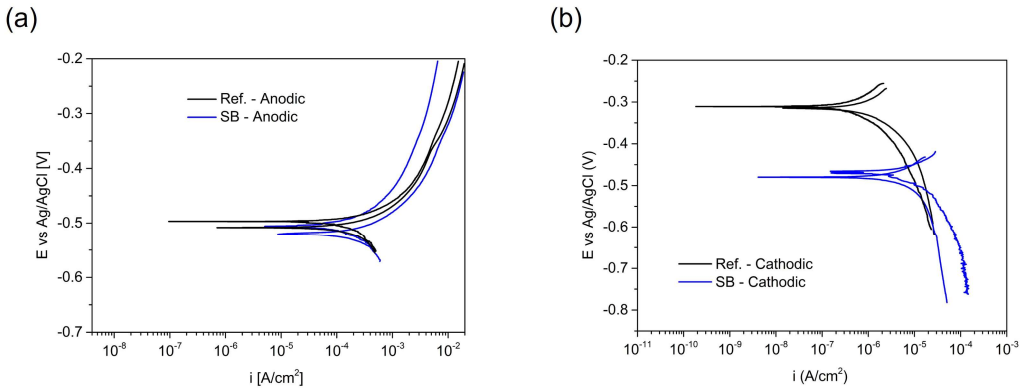

Figure A2. Replicas of the polarization curves obtained in the testing solutions simulating an anodic environment (**a**) and a cathodic one (**b**). PDPs collected on bare steel surface using anolyte and catholyte "Ref." with 3 g/L of SB added.

References

1. Trentin, A.; Pakseresht, A.; Duran, A.; Castro, Y.; Galusek, D. Electrochemical Characterization of Polymeric Coatings for Corrosion Protection: A Review of Advances and Perspectives. *Polymers* **2022**, *14*, 2306. https://doi.org/10.3390/polym14122306.
2. Lyon, S.B.; Bingham, R.; Mills, D.J. Advances in Corrosion Protection by Organic Coatings: What We Know and What We Would like to Know. *Prog. Org. Coat.* **2017**, *102*, 2–7. https://doi.org/10.1016/j.porgcoat.2016.04.030.
3. Grundmeier, G.; Schmidt, W.; Stratmann, M. Corrosion Protection by Organic Coatings: Electrochemical Mechanism and Novel Methods of Investigation. *Electrochim. Acta* **2000**, *45*, 2515–2533. https://doi.org/10.1016/S0013-4686(00)00348-0.
4. Pélissier, K.; Thierry, D. Powder and High-Solid Coatings as Anticorrosive Solutions for Marine and Offshore Applications? A Review. *Coatings* **2020**, *10*, 916. https://doi.org/10.3390/COATINGS10100916.
5. Cristoforetti, A.; Rossi, S.; Deflorian, F.; Fedel, M. Exploring the Role of Passivating Conversion Coatings in Enhancing the Durability of Organic-Coated Steel Against Filiform Corrosion Using an Electrochemical Simulated Approach. *Prog. Org. Coat.* **2024**, *189*, 108357. https://doi.org/10.1016/j.porgcoat.2024.108357.
6. Milošev, I.; Frankel, G.S. Review—Conversion Coatings Based on Zirconium and/or Titanium. *J. Electrochem. Soc.* **2018**, *165*, C127–C144. https://doi.org/10.1149/2.0371803jes.
7. Bastos, A.C.; Ferreira, M.G.; Simões, A.M. Corrosion Inhibition by Chromate and Phosphate Extracts for Iron Substrates Studied by EIS and SVET. *Corros. Sci.* **2006**, *48*, 1500–1512. https://doi.org/10.1016/j.corsci.2005.05.021.
8. Alibakhshi, E.; Ghasemi, E.; Mahdavian, M. Sodium Zinc Phosphate as a Corrosion Inhibitive Pigment. *Prog. Org. Coat.* **2014**, *77*, 1155–1162. https://doi.org/10.1016/j.porgcoat.2014.03.027.

9. Mahdavian, A.M.; Attar, M.M. Investigation on Zinc Phosphate Effectiveness at Different Pigment Volume Concentrations via Electrochemical Impedance Spectroscopy. *Electrochim. Acta* **2005**, *50*, 4645–4648. https://doi.org/10.1016/j.electacta.2005.02.015.
10. Prosek, T.; Thierry, D. A Model for the Release of Chromate from Organic Coatings. *Prog. Org. Coat.* **2004**, *49*, 209–217. https://doi.org/10.1016/j.porgcoat.2003.09.012.
11. Kalenda, P.; Kalendová, A.; Štengl, V.; Antoš, P.; Šubrt, J.; Kváča, Z.; Bakardjieva, S. Properties of Surface-Treated Mica in Anti-corrosive Coatings. *Prog. Org. Coat.* **2004**, *49*, 137–145. https://doi.org/10.1016/j.porgcoat.2003.09.003.
12. Saurbier, K.; Schultze, J.W.; Geke, J. Temporary Inhibitors of Corrosion in Wet Atmosphere: Electrochemical Investigations of the Mechanism and Efficiency. *Electrochim. Acta* **1994**, *39*, 1171–1178. https://doi.org/10.1016/0013-4686(94)E0033-V.
13. 14. Lahem, D.; Poelman, M.; Atmani, F.; Olivier, M.G. Synergistic Improvement of Inhibitive Activity of Dicarboxylates in Preventing Mild Steel Corrosion in Neutral Aqueous Solution. *Corros. Eng. Sci. Technol.* **2012**, *47*, 463–471. https://doi.org/10.1179/1743278212Y.0000000030.
14. Rocca, E.; Steinmetz, J. Inhibition of Lead Corrosion with Saturated Linear Aliphatic Chain Monocarboxylates of Sodium. *Corros. Sci.* **2001**, *43*, 891–902. https://doi.org/10.1016/S0010-938X(00)00115-3.
15. Georges, C.; Rocca, E.; Steinmetz, P. Synergistic Effect of Tolutriazol and Sodium Carboxylates on Zinc Corrosion in Atmospheric Conditions. *Electrochim. Acta* **2008**, *53*, 4839–4845. https://doi.org/10.1016/j.electacta.2008.01.073.
16. Boisier, G.; Lamure, A.; Pébère, N.; Portail, N.; Villatte, M. Corrosion Protection of AA2024 Sealed Anodic Layers Using the Hydrophobic Properties of Carboxylic Acids. *Surf. Coat. Technol.* **2009**, *203*, 3420–3426. https://doi.org/10.1016/j.surfcoat.2009.05.008.
17. Shulman, G.P.; Bauman, A.J. Organic Acid Sealants for Anodized Aluminum—A New Method for Corrosion Protection. *Met. Finish.* **1995**, *93*, 16–19. https://doi.org/10.1016/0026-0576(95)91305-7.
18. Hefter, G.T.; North, N.A.; Tan, S.H. Organic Corrosion Inhibitors in Neutral Solutions; Part 1—Inhibition of Steel, Copper, and Aluminum by Straight Chain Carboxylates. *Corrosion* **1997**, *53*, 657–667. https://doi.org/10.5006/1.3290298.
19. Ormellese, M.; Lazzari, L.; Goidanich, S.; Fumagalli, G.; Brenna, A. A Study of Organic Substances as Inhibitors for Chloride-Induced Corrosion in Concrete. *Corros. Sci.* **2009**, *51*, 2959–2968.
20. Rammelt, U.; Reinhard, G. Application of Electrochemical Impedance Spectroscopy (EIS) for Characterizing the Corrosion-Protective Performance of Organic Coatings on Metals. *Prog. Org. Coat.* **1992**, *21*, 205–226. https://doi.org/10.1016/0033-0655(92)87005-U.
21. Rammelt, U.; Koehler, S.; Reinhard, G. Electrochemical Characterisation of the Ability of Dicarboxylic Acid Salts to the Corrosion Inhibition of Mild Steel in Aqueous Solutions. *Corros. Sci.* **2011**, *53*, 3515–3520. https://doi.org/10.1016/j.corsci.2011.06.023.
22. Godinez-Alvarez, J.M.; Mora-Mendoza, J.L.; Rodriguez-Betancourt, E.; Zavala- Olivares, G.; Gonzalez-Nunez, M.A. Inhibition of Ferrous Metal Corrosion by Carboxylates.; New Orleans, Louisiana, March 28 2004.
23. Mayne, J.; Page, C. Inhibition of the Corrosion of Iron by Benzoate and Acetate Ions. *Br. Corros. J.* **1974**, *9*, 223–226.
24. Ochoa, N.; Moran, F.; Pébère, N. The Synergistic Effect between Phosphonocarboxylic Acid Salts and Fatty Amines for the Corrosion Protection of a Carbon Steel. *J. Appl. Electrochem.* **2004**, *34*, 487–493.
25. Caballero, D.; Beltrán-Cobos, R.; Tavares, F.; Cruz-Yusta, M.; Granados, L.S.; Sánchez-Moreno, M.; Pavlovic, I. The Inhibitive Effect of Sebacate-Modified LDH on Concrete Steel Reinforcement Corrosion. *ChemEngineering* **2022**, *6*, 72. https://doi.org/10.3390/chemengineering6050072.
26. Nguyen, D.T.; To, H.T.X.; Gervasi, J.; Paint, Y.; Gonon, M.; Olivier, M.G. Corrosion Inhibition of Carbon Steel by Hydrotalcites Modified with Different Organic Carboxylic Acids for Organic Coatings. *Prog. Org. Coat.* **2018**, *124*, 256–266. https://doi.org/10.1016/j.porgcoat.2017.12.006.
27. Bouali, A.C.; Serdechnova, M.; Blawert, C.; Tedim, J.; Ferreira, M.G.S.; Zheludkevich, M.L. Layered Double Hydroxides (LDHs) as Functional Materials for the Corrosion Protection of Aluminum Alloys: A Review. *Appl. Mater. Today* **2020**, *21*, 100857. https://doi.org/10.1016/j.apmt.2020.100857.
28. Cristoforetti, A.; Deflorian, F.; Rossi, S.; Fedel, M. On the Occurrence of Filiform Corrosion on Organic Coated Carbon Steel Exposed to Cyclic Aging Test. *Corrosion* **2023**, *79*, 1339–1344. https://doi.org/10.5006/4443.
29. Cristoforetti, A.; Izquierdo, J.; Souto, R.M.; Deflorian, F.; Fedel, M.; Rossi, S. In-Situ Measurement of Electrochemical Activity Related to Filiform Corrosion in Organic Coated Steel by Scanning Vibrating Electrode Technique and Scanning Micropotentiometry. *Corros. Sci.* **2024**, *227*, 111669. https://doi.org/10.1016/j.corsci.2023.111669.
30. Williams, G.; McMurray, H.N. The Mechanism of Group (I) Chloride Initiated Filiform Corrosion on Iron. *Electrochem. Commun.* **2003**, *5*, 871–877. https://doi.org/10.1016/J.ELECOM.2003.08.008.
31. Watson, T.M.; Coleman, A.J.; Williams, G.; McMurray, H.N. The Effect of Oxygen Partial Pressure on the Filiform Corrosion of Organic Coated Iron. *Corros. Sci.* **2014**, *89*, 46–58. https://doi.org/10.1016/j.corsci.2014.08.004.
32. Bautista, A. Filiform Corrosion in Polymer-Coated Metals. *Prog. Org. Coat.* **1996**, *28*, 49–58. https://doi.org/10.1016/0300-9440(95)00555-2.
33. Ruggeri, R.T.; Beck, T.R. An Analysis of Mass Transfer in Filiform Corrosion. *Corrosion* **1983**, *39*, 452–465. https://doi.org/10.5006/1.3581907.
34. Mol, J.M.C.; Hinton, B.R.W.; Van Der Weijde, D.H.; De Wit, J.H.W.; Van Der Zwaag, S. A Filiform Corrosion and Potentiodynamic Polarisation Study of Some Aluminium Alloys. *J. Mater. Sci.* **2000**, *35*, 1629–1639. https://doi.org/10.1023/A:1004795528090.
35. Cristoforetti, A.; Rossi, S.; Deflorian, F.; Fedel, M. An Electrochemical Study on the Mechanism of Filiform Corrosion on Acrylic-Coated Carbon Steel. *Prog. Org. Coat.* **2023**, *179*, 107525. https://doi.org/10.1016/j.porgcoat.2023.107525.

36. Pourbaix, M.; Burbank, J. Atlas D-Equilibres Electrochimiques. *J. Electrochem. Soc.* **1964**, *111*, 14C.
37. *ASTM D2803-09*; Standard Guide for Testing Filiform Corrosion Resistance of Organic Coatings on Metal. ASTM International: West Conshohocken, PA, USA, 2020.
38. *ASTM B117-19*; Standard Practice for Operating Salt Spray (Fog) Apparatus. ASTM International: West Conshohocken, PA, USA, 2019.
39. Cristoforetti, A.; Parola, F.; Parrino, F.; Izquierdo, J.; Souto, R.M.; Rossi, S.; Deflorian, F.; Fedel, M. Sebacate Intercalated CaAl Layered Double Hydroxide Pigments for Corrosion Protection of Low Carbon Steel: Anion Exchange and Electrochemical Properties. *Appl. Clay Sci.* **2024**, *250*, 107300. https://doi.org/10.1016/j.clay.2024.107300.
40. Fedel, M.; Poelman, M.; Olivier, M.; Deflorian, F. Sebacic Acid as Corrosion Inhibitor for Hot-Dip Galvanized (HDG) Steel in 0.1 M NaCl. *Surf. Interface Anal.* **2019**, *51*, 541–551. https://doi.org/10.1002/sia.6617.
41. Peng, Y.; Hughes, A.E.; Mardel, J.I.; Deacon, G.B.; Junk, P.C.; Catubig, R.A.; Forsyth, M.; Hinton, B.R.W.; Somers, A.E. Dual Function of Rare Earth Carboxylate Compounds on the Barrier Properties and Active Corrosion Inhibition of Epoxy Coatings on Mild Steel. *Prog. Org. Coat.* **2023**, *185*, 107870. https://doi.org/10.1016/j.porgcoat.2023.107870.
42. Catubig, R.; Seter, M.; Neil, W.; Forsyth, M.; Hinton, B. Effects of Corrosion Inhibiting Pigment Lanthanum 4-Hydroxy Cinnamate on the Filiform Corrosion of Coated Steel. *J. Electrochem. Soc.* **2011**, *158*, C353–C358. https://doi.org/10.1149/2.012111jes.
43. Glover, C.F.; Williams, G. Inhibition of Corrosion-Driven Organic Coating Delamination and Filiform Corrosion on Iron by Phenyl Phosphonic Acid. *Prog. Org. Coat.* **2017**, *102*, 44–52. https://doi.org/10.1016/J.PORGCOAT.2016.03.006.
44. Tokutake, K.; Nishi, H.; Ito, D.; Okazaki, S.; Serizawa, Y. Relationship between Degradation Characteristics of Organic Coating on Internal Bottom Plate of Oil Storage Tank and Constant-Phase Element Parameter Values. *Prog. Org. Coat.* **2015**, *87*, 69–74. https://doi.org/10.1016/j.porgcoat.2015.05.004.